[Frontiers in Bioscience, Landmark, 21, 178-191, January 1, 2016]

Caspase-1 mediates hyperlipidemia-weakened progenitor cell vessel repair

Ya-Feng Li[1], Xiao Huang[2,3,4], Xinyuan Li[3,4], Ren Gong[2,3,4], Ying Yin[3,4], Jun Nelson[3,4], Erhe Gao[5], Hongyu Zhang[4], Nicholas E. Hoffman[5], Steven R. Houser[4], Muniswamy Madesh[5], Douglas G. Tilley[5], Eric T. Choi[3], Xiaohua Jiang[3,4], Cong-Xin Huang[1], Hong Wang[3,4], Xiao-Feng Yang[3,4]

[1]Department of Cardiology, Renmin Hospital of Wuhan University, Wuhan, Hubei Province 430060, China, [2]Department of Cardiology, The Second Affiliated Hospital to Nanchang University, Nanchang, JiangXi 330006, China, [3]Center for Metabolic Disease Research, Department of Pharmacology, Thrombosis Research Center, [4]Cardiovascular Research Center, [5]Center for Translational Medicine, Department of Surgery, Temple University School of Medicine, Philadelphia, PA 19140, USA

TABLE OF CONTENTS

1. ABSTRACT

Caspase-1 activation senses metabolic danger-associated molecular patterns (DAMPs) and mediates the initiation of inflammation in endothelial cells. Here, we examined whether the caspase-1 pathway is responsible for sensing hyperlipidemia as a DAMP in bone marrow (BM)-derived Stem cell antigen-1 positive (Sca-1$^+$) stem/progenitor cells and weakening their angiogenic ability. Using biochemical methods, gene knockout, cell therapy and myocardial infarction (MI) models, we had the following findings: *1)* Hyperlipidemia induces caspase-1 activity in mouse Sca-1$^+$ progenitor cells *in vivo*; *2)* Caspase-1 contributes to hyperlipidemia-induced modulation of vascular cell death-related gene expression *in vivo*; *3)* Injection of Sca-1$^+$ progenitor cells from caspase-1$^{-/-}$ mice improves endothelial capillary density in heart and decreases cardiomyocyte death in a mouse model of MI; and 4*)* Caspase-1$^{-/-}$ Sca-1$^+$ progenitor cell therapy improves mouse cardiac function after MI. Our results provide insight on how hyperlipidemia activates caspase-1 in Sca-1$^+$ progenitor cells, which subsequently weakens Sca-1$^+$ progenitor cell repair of vasculature injury. These results demonstrate the therapeutic potential of caspase-1 inhibition in improving progenitor cell therapy for MI.

2. INTRODUCTION

Cardiovascular diseases (CVDs) including myocardial infarction and stroke are the number one cause of death in US and globally. Dyslipidemia/hyperlipidemia,

an independent risk factor for cardiovascular diseases (CVDs), is defined as pathologically elevated plasma concentrations of cholesterol and other lipids (1). Reports from our lab and others support the idea that hyperlipidemia, along with other risk factors such as glucose and homocysteine, promotes CVDs via several mechanisms including inducing endothelial activation and injury (2-4), increasing monocyte differentiation and recruitment (5-8), decreasing the population of regulatory T cells (9,10), and impairing the vascular repair ability of bone marrow (BM)-derived progenitor cells (11).

The roles of the pattern recognition receptors (PRRs) for pathogen-associated molecular patterns (PAMPs) have recently been characterized as bridging the sensing systems for host defense against the invasion of infectious agents and uncontrolled metabolic stress including dyslipidemia/hyperlipidemia (danger signal-associated molecular patterns, DAMPs) to the initiation of inflammation. Among PRRs, the Toll-like receptors (TLRs) recognize a variety of conserved microbial PAMPs/DAMPs. In addition, TLRs also work in synergy with cytosolic sensing receptor families including NLRs (NOD (nucleotide binding and oligomerization domain)-like receptors) in recognizing endogenous metabolic stress-derived DAMPs to upregulate and activate a range of inflammatory genes (12). Pro-caspase-1 is present in the cytosol as an inactive zymogen and requires the assembly of a NLR-containing protein complex termed "inflammasome" for activation. Caspase-1 activation is subsequently required for the maturation of proinflammatory cytokines including pro-interleukin-1β (IL-1β) and pro-IL-18. Previous reports showed that hyperlipidemia stimuli cholesterol crystals formed in the advanced stage of atherosclerosis (13) activate the NLRP3 (NLR family, pyrin domain containing 3) inflammasome in BM-derived macrophages, which is required for atherogenesis (14,15). In addition, we have reported that NLRP3 inflammasome is not constitutively expressed in vascular tissue (16); and that early hyperlipidemia promotes endothelial activation and early atherosclerosis development via a caspase-1-sirtuin 1 pathway (4). However, an important question remains that whether the caspase-1 pathway is responsible for sensing hyperlipidemia as a DAMP in BM-derived progenitor cells, which contributes to hyperlipidemia-induced impairment of vascular cell repair.

In this study, we examined the hypothesis that the caspase-1 pathway in BM-derived Sca-1^+ progenitor cells can sense dyslipidemia and that caspase-1 activation in Sca-1^+ progenitor cell impairs their angiogenic ability during ischemic injury. To examine this hypothesis, we examined caspase-1 activity in mouse Sca-1^+ progenitor cells in atherogenic apolipoprotein E deficient (ApoE$^{-/-}$) mice after high fat (HF) diet feeding *in vivo*. We also performed cDNA microarray analysis to determine the downstream effects of hyperlipidemia-induced caspase-1 activation *in vivo*. In addition, we utilized a mouse model of myocardial infarction (MI) to determine whether caspase-1 gene depletion could enhance the therapeutic efficacy of progenitor cell therapy in ischemic myocardium. Our results demonstrate that caspase-1 activation is responsible for hyperlipidemia-induced vascular dysfunction by impairing vessel repair f of Sca-1^+ progenitor cells.

3. MATERIALS AND METHODS

3.1. Reagents

EGM-2 Medium was purchased from Lonza corporation (CC-3202). Histopaque®-1083 was from Sigma-Aldrich (10831). FAM-YVAD-FMK caspase-1 detection kit was from Cell Technology (FAM600-2). Anti-APC MultiSort kit and MicroBeads were from MACS (130-091-255/130-048-801). Rat IgG2a K Isotype control APC was from eBioscience (17-4321-81). Biotinylated Griffonia simplicifolia lectin I (isolectin B4) from Vector (B-1205), Biotin-XX conjugate was from Invitrogen (I21414). APC anti-mouse Ly-6A/E (Sca-1) antibody were from Biolegend (121906/108112). All other reagents were purchased from Sigma-Aldrich (St. Louis, MO).

3.2. Mice and diets

All mice were in a C57B/L6 strain background. Wild-type (WT) and ApoE$^{-/-}$ mice were purchased from the Jackson Laboratories (Bar Harbor, Maine). Caspase $1^{-/-}$ mice were generously provided by Dr. Flavell's laboratory (Department of Immunobiology, Yale University School of Medicine) (17). ApoE/caspase-1 double gene deficient (ApoE$^{-/-}$/caspase-$1^{-/-}$) mice were generated by crossing caspase-$1^{-/-}$ mice into ApoE$^{-/-}$ mice as we reported (4). Male mice were fed either standard rodent chow diet (catalog #8640; Harlan Teklad, Madison, WI) or HF diet (catalog #88137, Harlan Teklad) starting from 8 weeks to induce dietary dyslipidemia as we reported (4). All mouse protocols were approved by the Temple University Institutional Animal Care and Use Committee.

3.3. Transcriptome microarray analysis

Total RNA was extracted from the aortas of mice using the RNeasy Kit (Qiagen, Valencia, CA). RNA quantity was determined by the NanoDrop ND-2000 (Thermo Scientific, Wilmington, DE). The RNA integrity was determined by the RNA 28S/18S ratio using the Agilent 2100 Bioanalyzer (Agilent Technologies, Santa Clara, CA). Then samples were labeled and hybridized to the Affymetrix Genechip Mouse Gene 2.0.ST Arrays (Santa Clara, CA) following the manufacturer's instructions at the Expression Microarray Core Facility in the Fox Chase Cancer Center, Temple University. Scanned microarray images were analyzed using the Affymetrix Gene Expression Console with Robust Multi-array Average normalization algorithm.

3.4. Microarray data analysis

Our affymetrix data analysis was done in the R statistical environment using "oligo" and "limma" packages.

Venn diagram analysis was performed in the R statistical environment using the package "VennDiagram". Heat map and scatter plot were performed using the statistical tools provided by the R and Bioconductor projects.

3.5. Ingenuity pathway analysis

In order to categorize clinical functions and molecular and cellular functions related to the identified genes in our microarray analysis, the Ingenuity Pathway Analysis (IPA, Ingenuity Systems, www.ingenuity.com) was used. The differentially expressed genes were identified and uploaded into IPA for analysis. The IPA Tox analysis was used for clinical pathology functions and the Core analysis was used for molecular and cellular pathways.

3.6. Flow cytometry analysis of Sca-1$^+$ cells

After mouse BM was harvested from the femurs and tibiae, the collected cells were added with ACK buffer to lysis red blood cells and homogenized into a single cell suspension afterwards by mixing and filtering through a 70 micron filter. After centrifugation, cells were washed and resuspended in EGM-2 medium. Active caspase-1 levels were determined with APO LOGIX kit (Cell Tech., Mountain View, CA). The kit contains a carboxyfluorescein (FAM)(Excitation/Emission (nm):490/520)-labeled peptide fluoromethyl ketone (FMK) caspase-1 inhibitor (FAMYVAD-FMK), which enters the cell and irreversibly binds to activated caspase-1 but not pro-caspase-1. All procedures were performed according to the manufacturer's instruction. Briefly, cell suspension were incubated at 37°C with 1 x FAM-YVAD-FMK for 1 hour and then washed with 1x washing buffer. For the cell surface marker Sca-1 staining, cells were incubated for 30 minutes with monoclonal antibody against mouse Sca-1 or isotype control. Cells were washed afterwards and fixed in 2% paraformaldehyde before flow cytometry analysis. The data were analyzed by LSR II flow cytometer (BD Biosciences, San Jose, CA) and the FlowJo software (Tree Star, Ashland, OR).

3.7. Magnetic cell sorting and cell trace of Sca-1$^+$ cells

BM-derived mononuclear cells were isolated from the BM of WT mice or caspase-1$^{-/-}$ mice by density gradient using Histopaque-1083. Sca-1$^+$ cells were purified by an autoMACS separator (Miltenyi Biotec), using magnetic beads-coated mouse APC anti-mouse Ly-6A/E (Sca-1) antibody and an Anti-APC MultiSort Kit according to the manufacturer's instructions. To evaluate the homing of injected cells to infarcted heart, purified Sca-1$^+$ cells were labeled with CellVue^R NIR (near-infrared) 780 (Excitation max: 745nm/Emission max: 776nm, Mol. Targeting Tech. Inc. West Chester, PA) and injected peri-orbitally into C57/B6 mice, 6 hours before MI procedure. Images for tracing CellVue^R NIR-labelled Sca-1$^+$ cells were performed using the Multispectral FX Pro (Fixed Lens) Image Station (Carestream Health, Woodbridge, CT) for near-infrared fluorescence (NIRF) signals both prior to and at 0, 21, 24 and 45 hours post-CellVue^R and post-PSVue injection.

3.8. Experimental MI and cell therapy

Experiments were performed in 14-16 weeks old male WT mice fed a HF diet for 6 weeks. Acute MI was induced by permanent left anterior descending coronary artery ligation as previously described (18). Briefly, mice were anesthetized with 2% isoflurane. A skin incision was made over the left thorax, and the pectoral muscles were retracted to expose the ribs. At the level of the fourth intercostal space, the heart was exposed and pumped out through an expanded space between ribs. After a permanent knot was made around the left anterior descending coronary artery (LAD) at 2–3 mm from its origin with 6-0 silk suture, the heart was immediately placed back into the intrathoracic space, followed by manual evacuation of pneumothoraces and closure of the incision. Sham-operated animals were subjected to the same surgical procedures except that the suture was passed under the LAD but was not tied. After full recovery from cardiac surgery (four hours after MI), animals were randomized into two cell therapy groups. Purified Sca-1$^+$ cells were injected peri-orbitally into those mice.

3.9. Measurement of cardiac function

Mouse cardiac function was measured with echocardiography (ECHO). ECHO was performed with VisualSonics Velvo 770 high-resolution *in vivo* micro-imaging system (FUJIFILM VisualSonics, Toronto, Canada). Mice were anesthetized with 2% isoflurane initially and then 1% during the ECHO procedure. Hearts were examined in the short-axis between the two papillary muscles of the left ventricle (LV) and analyzed in M-mode. The parameters of cardiac function were measured offline with the Velvo 770 software including LV end diastolic diameter (EDD), end-systolic diameter (ESD), posterior wall thickness (PWT), and septal wall thickness (SWT) to determine cardiac morphological changes and ejection fraction (EF), heart rate and fractional shortening (FS). The EF and FS were calculated as reported (19).

3.10. TUNEL assay

Apoptotic cells were detected by terminal deoxynucleotidyl transferase-mediated nick-end labeling (TUNEL) using the APO-BrdU TUNEL Assay Kit (Millipore) as per the manufacturer's protocol. Briefly, Hearts were embedded in OCT media (Sakura Finetechnical Co., Ltd. Japan). Frozen ventricular sections (5 μm) were fixed in 4% (w/v) paraformaldehyde for 15 min on ice, permeabilized with 70% ethanol for 30 min on ice, and incubated with 50 μL DNA-labeling solution containing TdT enzyme and Br-dUTP at 37°C for 60 min. After the labeling reaction, the sections were washed and stained with fluorescein-labeled anti-BrdU antibody for 30 min. Before mounting, the cells were stained with 4′, 6-diamidino-2-phenylindole (DAPI) and Alexa Fluor 594-labeled phalloidin (Invitrogen). Images were

captured using a Zeiss 710 confocal microscope, 63 x oil objective, 1.4. x digitial zoom with excitations at 405, 488, and 594 for nuclei, TUNEL, and phalloidin, respectively. The percentage of TUNEL positive cells was quantitated using Image J (NIH) from 4–5 regions per heart, and an area of at least 100 cardiac myocytes.

3.11. Capillary density assay

Mouse hearts were removed at two weeks after MI and kept at -80°C until histological analysis. Frozen heart tissues were cut into 5 μm thick slices. Adjacent sections (taken at the midpoint between LAD ligation site and apex) were stained with Biotinylated Griffonia simplicifolia lectin I (isolectin B4) to stain endothelial cells in neovasculature from the mouse myocardial infarcted heart section (20). Images were captured using a Zeiss 710 confocal microscope using a 63 x oil objective and 1.4. x digital zoom with excitations at 405 and 594 for nuclei and IB4, respectively. Capillary density was expressed as $IB4^+$ endothelial cells per field.

3.12. Data analysis

All the experiments were performed at least twice, and results were expressed as the mean ± standard error (S.E.). Statistical comparison of single parameters between two groups was performed by paired Student *t* test. One-way ANOVA was used to compare the means of multiple groups. Data were considered statistically significant if *p* was <0.0.5.

4. RESULTS

4.1. Hyperlipidemia increases caspase-1 activity in Sca-1^+ progenitor cells

We and the others have shown previously that caspase-1 activation is responsible for hyperlipidemia-induced endothelial cell activation and macrophage inflammation (4,14,15). However, the question of whether caspase-1 is activated in Sca-1^+ progenitor cells in response to hyperlipidemia remained unknown. We hypothesized that Sca-1^+ progenitor cells also had a functional inflammasome pathway, which could sense hyperlipidemia and activate caspase-1. To test this hypothesis, we measured caspase-1 activity in BM-derived Sca-1^+ progenitor cells after hyperlipidemia challenge. We collected BM cells from WT mice and $ApoE^{-/-}$ mice fed with either chow diet or HF diet for 12 weeks and prepared single cell suspensions for flow cytometry analysis (Figure 1A). Within the mononuclear cell populations of BM, we gated Sca-1^+ progenitor cells to measure their caspase-1 activity (Figure 1B). We found that when compared with either $ApoE^{-/-}$ mice or WT mice fed with chow diet, HF diet feeding significantly increased caspase-1 activity in mouse Sca-1^+ progenitor cells ($p<0.0.5$) (Figure 1C), suggesting that at least one type of NLR inflammasomes and caspase-1 are fully expressed/functional in progenitor cells and could be post-translationally activated by hyperlipidemia stimuli.

4.2. Caspase-1 contributes to hyperlipidemia-induced modulation of vascular cell death gene expression

A recent report showed that stem cells/endothelial progenitor cells were present at low levels in mouse organs with the highest levels in adipose and aorta (21). To determine the functional effects of hyperlipidemia-induced caspase-1 activation in Sca-1^+ progenitor cells in mouse aortic context related to hyperlipidemia diseases, we performed cDNA microarray analysis in WT mice, $ApoE^{-/-}$ mice, and $ApoE^{-/-}$Caspase-$1^{-/-}$ mice fed with 3 weeks of HF diet. Since we have found that caspase-1 serves as a hyperlipidemia sensor during early hyperlipidemia (4), use of three-week HF diet feeding is justified. Of note, at this age of mice, plasma cholesterol triples in both $ApoE^{-/-}$ and $ApoE^{-/-}$Caspase-$1^{-/-}$ mice when compared with that in WT mice (4,22,23). This allows us to identify genes whose RNA expressions are changed in response to hyperlipidemia ($ApoE^{-/-}$ mice compared with WT mice) and identify how many genes whose RNA expressions are changed in response to hyperlipidemia can be reversed by caspase-1 gene deletion ($ApoE^{-/-}$Caspase-$1^{-/-}$ mice compared with $ApoE^{-/-}$ mice) (Figure 2). We found that among 23,470 genes that could be detected by the microarray analysis, 6,745 genes were significantly changed in response to hyperlipidemia, while 2,541 genes were significantly changed in response to caspase-1 gene deletion (Figures 3A and 3C). More importantly, most of the genes that were induced by hyperlipidemia could be significantly down-regulated by caspase-1 deficiency (Figure 3B). Moreover, among 6,745 differentially expressed genes induced by hyperlipidemia, 969 genes could be reversed by caspase-1 deficiency (Figures 3C). Interestingly, IL-1β, the proteolytic substrate of caspase-1, was among the most significantly decreased genes besides caspase-1 after caspae-1 deficiency (Figure 3D). This result suggested that caspase-1 could also transcriptionally up-regulate IL-1β gene expression independent from its well-characterized enzymatic cleavage activity. In addition, we found that apoptosis-related gene caspase-4 was among the genes that decreased the most after caspase-1 deficiency, suggesting that caspase-1 also promotes apoptosis (programmed cell death) besides its ability to induce pyroptosis (inflammatory cell death). Moreover, a group of different microRNAs (Mir) such as Mir 145 and Mir 143 were among the most significantly increased genes after caspase-1 gene deficiency instead, which suggested that caspase-1 could negatively affect regulatory non-coding RNA gene expressions, thereby contributing to epigenetic regulation of gene expression changes.

To identify the functional pathways of the pathological effects of Caspase 1 in hyperlipidemia, we analyzed the signatures of the 969 genes regulated by caspase-1 deficiency using IPA software. When we

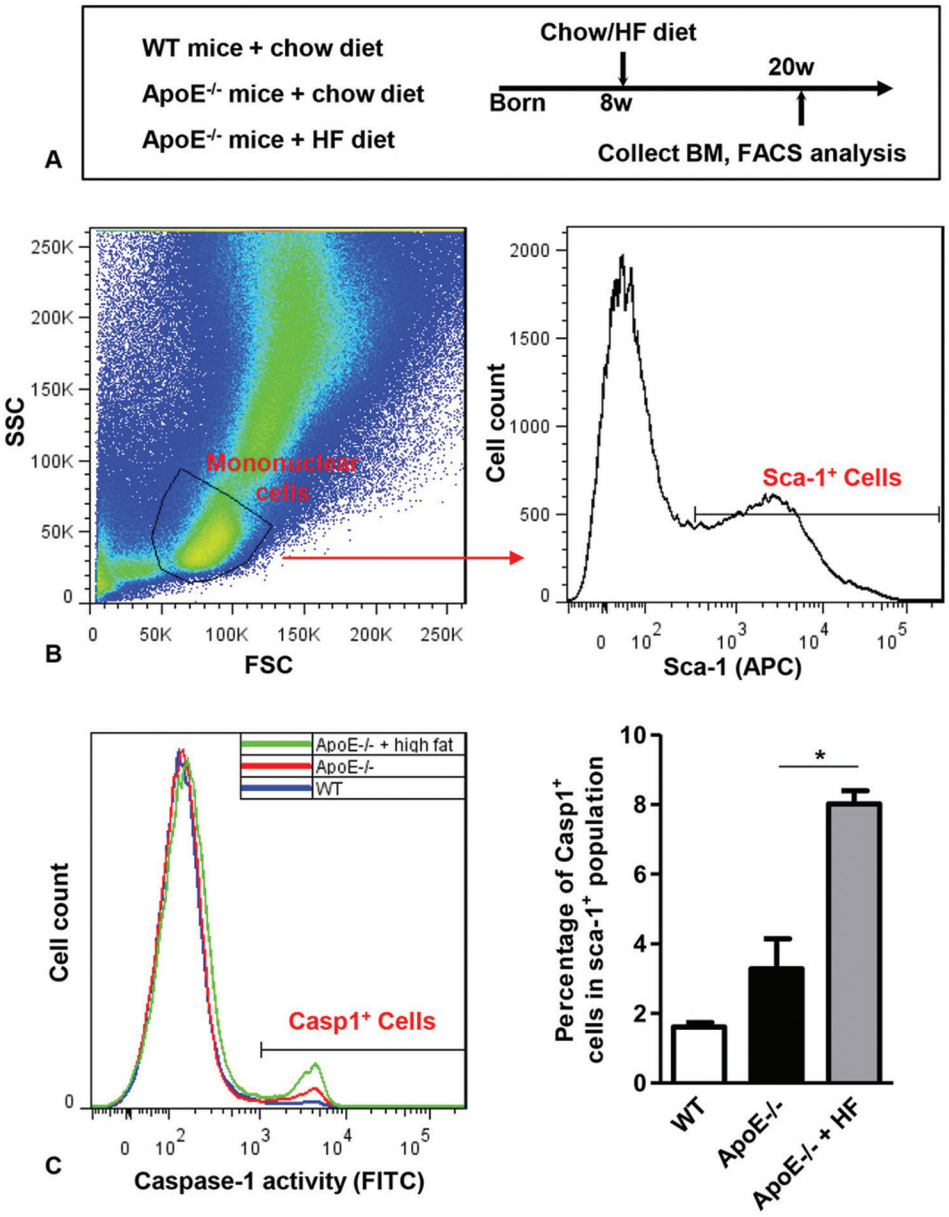

Figure 1. Hyperlipidemia increases caspase-1 activity in Sca-1$^+$ progenitor cells. A. Experiment design. Wild-type (WT) mice and ApoE$^{-/-}$ mice were fed with either chow diet or high fat (HF) for 12 weeks (w) before their bone marrows (BM) were collected for fluorescence activated cell sorter (FACS) analysis. B. After gating mononuclear cells from the BM, Sca-1$^+$ stem cells were gated from the mononuclear cells. C. Among Sca-1$^+$ stem cell populations in the BM, caspase-1 activity was measured. Gating of caspase-1 positive (Casp1$^+$) cells in Sca-1$^+$ population of mouse BM was shown in the left. Quantification was shown in the right.

examined top molecular pathways that were regulated by caspase-1 in hyperlipidemia condition, "Cellular Growth and Proliferation", "Cell Death and Survival" were the top two pathways identified, suggesting that hyperlipidemia-induced caspase-1 regulates vascular cell death (Figure 3E). In addition, we identified 13 genes associated with apoptosis and necrosis of endothelial cells that are regulated by hyperlipidemia-induced caspase-1 activation, such as tumor necrosis factor (TNF) super family members including tumor necrosis factor (ligand) superfamily member 10 (TNFSF10) and Fas ligand (FASLG), matrix degradation enzyme metallopeptidase 9 (MMP9), and mitogen-activated protein kinase (MAPK) family member MAP3K5 (Figure 3F). When we chose clinical endpoints as the readouts in our IPA analysis, we found that "Cardiac Hypertrophy" and "Increase Heart Failure" were among the top pathways that are regulated by hyperlipidemia-induced caspase-1 activation

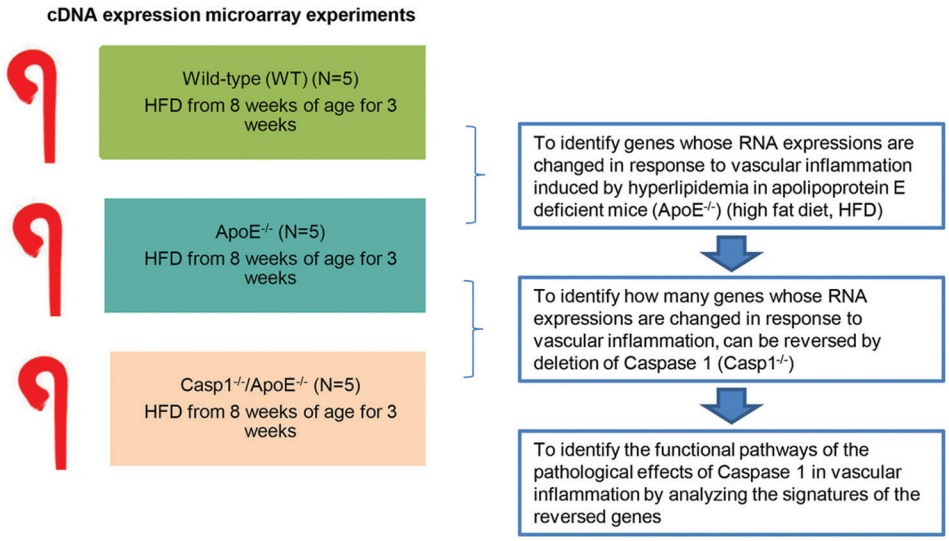

Figure 2. Flow chart of experiment design that was used for cDNA microarray analysis.

(Figure 4). Although mouse aortas instead of heart were used in our analysis, caspase-1 might mediate hyperlipidemia-induced cardiac dysfunction and hypoxia-triggered damage by inducing vascular cell death in these tissues.

4.3. Caspase-1$^{-/-}$ Sca-1^{+} progenitor cell therapy improves cardiac function after MI

Based on our results above that that dyslipidemia increases caspase-1 activity in Sca-1^{+} progenitor cells; and that caspase-1 contributes to the regulation of hyperlipidemia-induced vascular cell death, we hypothesized hyperlipidemia-induced caspase-1 activation in Sca-1^{+} progenitor cells leads to vascular cell damage by impairing their vessel repair capacity. To test this hypothesis, we compared the angiogenesis capacity of purified Sca-1^{+} cells from WT mice and those purified from caspase-1 deficient mice in a mouse model of MI (24). We used four groups of mice, *(i)* the mock-MI control group (n=13), *(ii)* the MI with no cell therapy control group (n=4), *(iii)* the MI with WT Sca-1^{+} progenitor cell therapy group (n=5), and *(iv)* the MI with caspase-1$^{-/-}$ Sca-1^{+} progenitor cell therapy group (n=5). As shown in Figure 5A, we first pre-conditioned the mice with a six week HF diet feeding (from day -42 to day 0). Sca-1^{+} progenitor cells were purified using a magnetic Sca-1^{+} cell purification column, and Sca-1^{+} cells were enriched from 35.5.% to as high as 85.4.% after the purification (Figure 5A). Then, we performed experimental acute MI procedures at the day 0 (18), to the three groups of the recipient mice, followed by Sca-1^{+} progenitor cell therapy (2 x 10^{6} cells/mouse). The numbers of transferred Sca-1+ progenitor cells were similar to 1 x 10^{6} BM-derived cells per mouse in a previous report (25). After MI, the control mice received purified WT Sca-1^{+} progenitor cells and the experimental mice received caspase-1$^{-/-}$ Sca-1^{+} purified progenitor cells. To ensure that Sca-1^{+} progenitor cells migrate to the acute MI lesion site, we used CellVue® NIR780-labelled Sca-1^{+} progenitor cells (2 x 10^{6} cells/mouse, n=4) to perform adoptive transfer to trace the Sca-1^{+} progenitor cell migration. 45 hours after the injection, we found that the CellVue® NIR780 near-infrared labeled Sca-1^{+} progenitor cells mostly migrated to the infarcted heart (Figure 5B). To examine whether caspase-1$^{-/-}$ Sca-1^{+} progenitor cell therapy has an enhanced therapeutic effects, we performed cardiac function analysis one day before MI and 14 days after MI using the M-mode echocardiography. The M-mode tracings presented in Figure 5C were obtained from WT mice without MI (control) and with MI using a 13 MHz transducer with the depth from 0 to -1 cm for 500 milliseconds as reported (26). The ejection fraction (EF) and fractional shortening (FS) are two commonly examined cardiac functions assayed by the M-mode echocardiography. As shown in Figure 5D left panel, the ejection fraction in the mouse group receiving caspase-1$^{-/-}$ Sca-1^{+} progenitor cell therapy was increased to 39.9.% from 23% in the mouse group receiving WT Sca-1^{+} progenitor cell therapy control (p<0.0.5). Similarly, the faction shorten index (Figure 5D right panel) in the mouse group receiving caspase-1$^{-/-}$ Sca-1^{+} progenitor cell therapy was also increased to 19.5.% from 10.4.% in the mouse group receiving WT Sca-1^{+} progenitor cell therapy control (p<0.0.5). These results suggest that caspase-1$^{-/-}$ Sca-1^{+} progenitor cell therapy significantly improves cardiac function compared to WT Sca-1^{+} progenitor cell therapy. In addition, we also examined

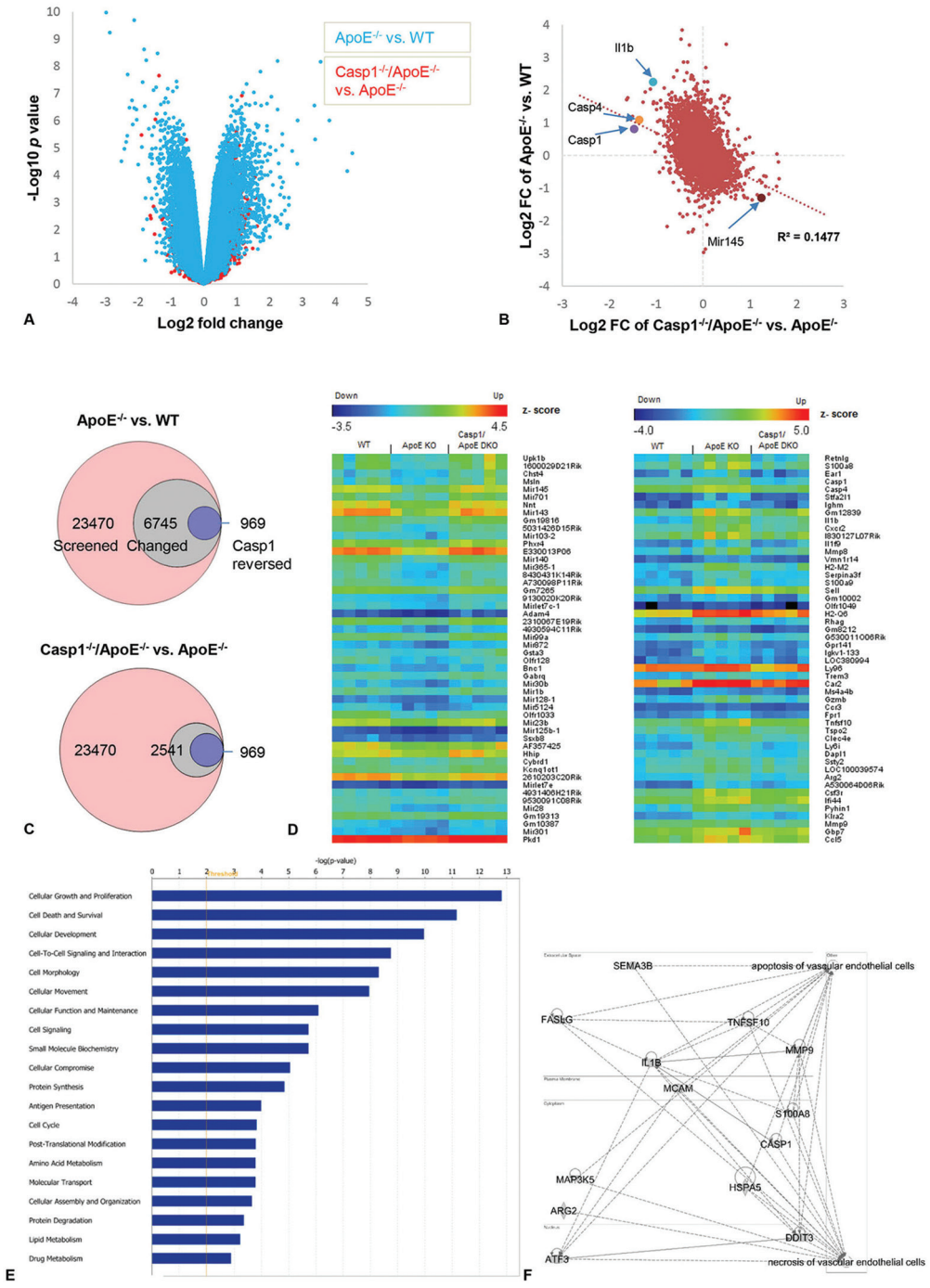

Figure 3. Caspase-1 contributes to hyperlipidemia-induced gene changes related to vascular cell death. A. Volcano plots of apoliprotein E deficient ($ApoE^{-/-}$) mice versus Wild type (WT) mice aorta DNA expression comparisons (blue), with the overlay of Caspase-1 $(Casp1)^{-/-}/ApoE^{-/-}$ versus $ApoE^{-/-}$ comparisons (red) are depicted by estimated fold change (FC)(log2 FC, x-axis) and statistical significance (–log10 P value, y-axis). B. Cooperation between Caspase1 and hyperlipidemia is shown by Log2 FC/Log2 FC plot comparing gene expression value for Caspase1/ApoE DKO versus ApoE KO (x-axis), and parallel ApoE KO versus WT (y-axis). C. Venn diagram shows the profile of two gene expression comparisons. Among 23,470 mapped genes, a total of 6,745 genes were significantly changed induced by hyperlipidemia and 2,541 genes were significantly changed caused by Caspase1 deletion. Among the changed genes, there are 969 genes changed in condition of hyperlipidemia and reversed by Caspase1 deletion. D. The heat-maps represent the z-score of the expression level of top 50 reversed genes (hyperlipidemia increased or decreased genes which are down-regulated or up-regulated by deletion of Caspase1). E. Core analysis with Ingenuity pathway analysis (IPA) shows that the major molecular and cellar functional pathways are cellular growth and proliferation and cell death. F. The network show the connection of the caspase-1 reserved genes associated with apoptosis and necrosis of endothelial cells.

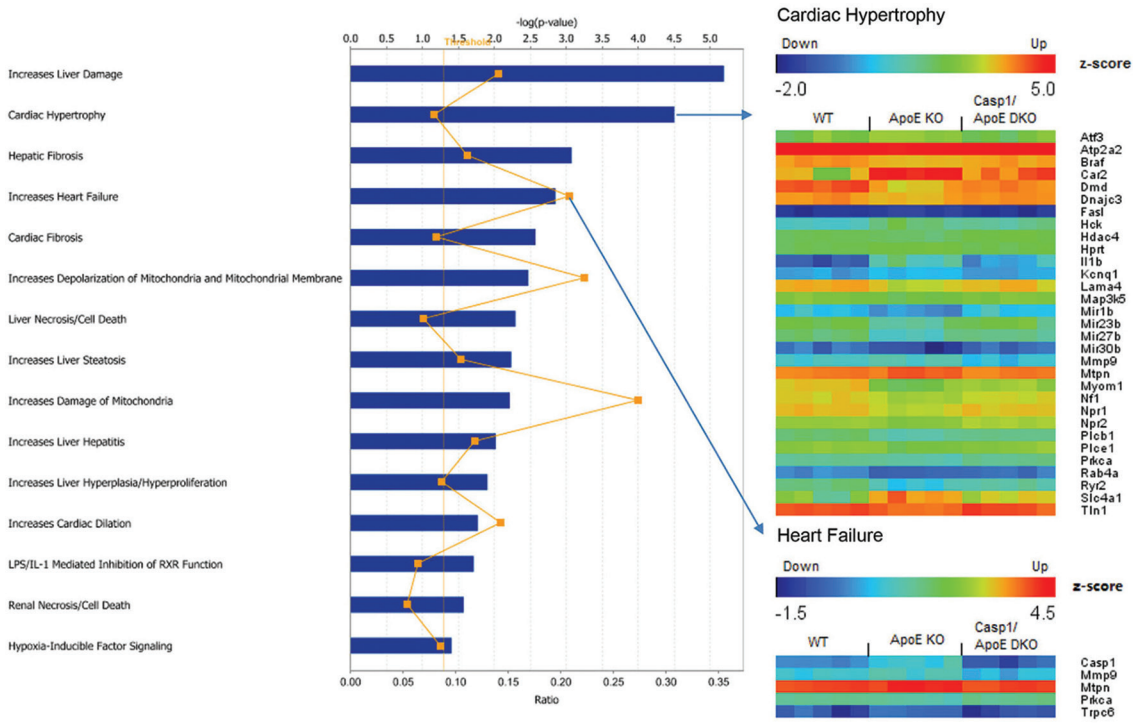

Figure 4. Caspase-1 contributes to hyperlipidemia-induced gene changes related to heart dysfunction. A. Tox analysis with Ingenuity pathway analysis (IPA) shows that the clinical pathology endpoints of these reversed genes. Heart hypertrophy and heart failure are the top endpoints associated with cardiovascular disease. Heat-maps showing the expression level of the involved genes in each endpoint are listed in the right.

the heart weight/body weight ratios, lung weight/body weight ratios and liver weight/body weight ratios in the three MI groups. As shown in Figure 5E, the heart weight/body weight ratios and liver weight/body weight ratios were not significantly changed among three MI groups. In contrast, the lung weight/body weight ratios in the caspase-$1^{-/-}$ Sca-1^{+} progenitor cell therapy group were significantly decreased to 0.0.075 from 0.0.119 (WT Sca-1^{+} cell therapy) and 0.0.094 (no cell therapy control)(p<0.0.5). The results suggest that the improved cardiac function in caspase-$1^{-/-}$ Sca-1^{+} progenitor cell therapy group may have relieved lung congestion and edema. Taken together, our results suggest that caspase-$1^{-/-}$ Sca-1^{+} progenitor cell therapy significantly improves cardiac function.

4.4. Caspase-$1^{-/-}$ Sca-1^{+} progenitor cell therapy improves endothelial capillary density and decreases cardiomyocyte cell death in the infarcted heart zone after MI

To determine the mechanisms underlying the beneficial effects of caspase-$1^{-/-}$ Sca-1^{+} progenitor cell therapy, we then hypothesized that the enhanced regenerative capacity of caspase-$1^{-/-}$ Sca-1^{+} progenitor cell therapy resulted from improved neovasculature formation and reduced cardiac myocyte cell death in comparison to the mice receiving WT Sca-1^{+} progenitor cells. To test this hypothesis, we examined whether mouse hearts receiving caspase-$1^{-/-}$ progenitor cell therapy have higher endothelial capillary density after MI than mouse hearts receiving WT Sca-1^{+} cell therapy using IB4 to stain endothelial cells in neovasculature from the infarcted heart sections (20). The immunohistochemistry results in Figure 6A showed that the infarcted heart section from the mice receiving caspase-$1^{-/-}$ Sca-1^{+} progenitor cell therapy have higher numbers of IB4^{+} endothelial cells than that of untreated MI hearts and that of the MI mice receiving WT Sca-1^{+} progenitor cell therapy. The fold change of IB4+ endothelial cell numbers in caspase-$1^{-/-}$ Sca-1^{+} progenitor cell therapy group over no treatment MI group is 1.3.1 (p<0.0.5). Then, we examined whether the enhanced angiogenesis in the MI lesion area of mice receiving caspase-$1^{-/-}$ Sca-1^{+} progenitor cell therapy leads to the reduction of cardiomyocyte cell death using TUNEL assay. The results in Figure 6B showed that the infarcted heart sections from the mice receiving caspase-$1^{-/-}$ Sca-1^{+} progenitor cell therapy have lower numbers of TUNEL^{+} cardiomyocytes (14.9.%) than that of untreated MI hearts (30.8.%) and that of the MI mouse hearts receiving WT Sca-1^{+} progenitor cell therapy (25.1.%)(p<0.0.5). Taken together, our results suggest that caspase-$1^{-/-}$ Sca-1^{+} progenitor cell therapy improves cardiac function from enhanced angiogenesis and reduction of cardiomyocyte cell death after MI.

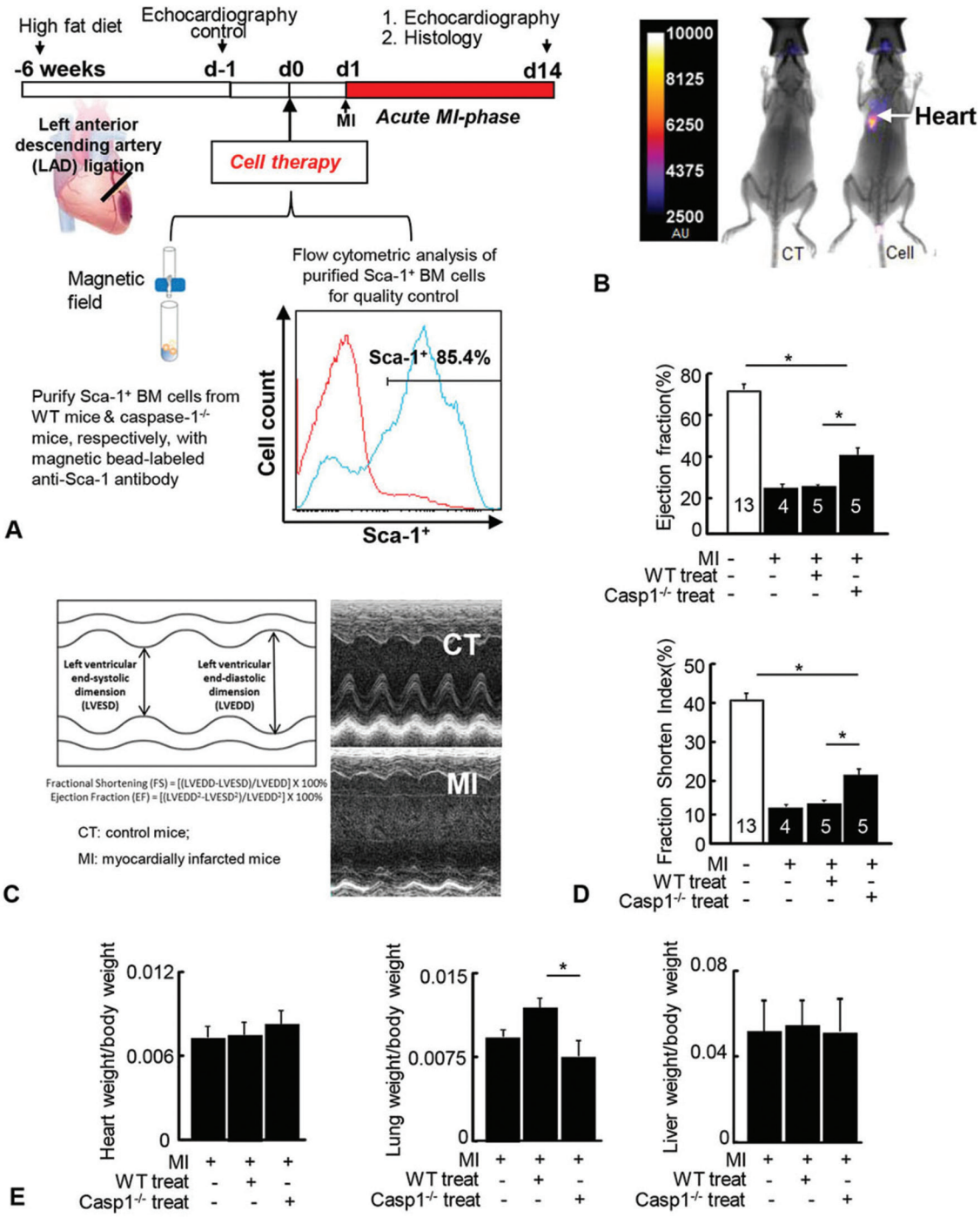

Figure 5. Caspase-1$^{-/-}$ Sca-1^{+} progenitor cell therapy improves cardiac function after MI. A. Myocardiac infarction (MI) and cell therapy model. Schematic representation of experimental plan including high fat diet feeding, cardiac function monitoring with echocardiography, cell therapy with purified Sca-1+ bone marrow cells followed by immunohistochemistry and flow cytometry analyses. B. The CellVue^{R} NIR780 fluorescence-labeled cells were traced to heart after intravenous injection. The CellVue^{R} NIR780 fluorescence-labeled purified Sca-1^{+} bone marrow cells (2 x 10^{6} cells/mouse) were traced to mouse heart after cell therapy (n=4 for tracer group, n=2 for non-cell tracer group). CT: no cell therapy control; cell: cell therapy C. M-mode Echocardiography. Representative M-mode echocardiographs of control mice and myocardiac infarcted mice. D. Cardiac functions measured with echocardiography. The cardiac function measurements of control mice, myocardial infarction (MI) mice, mice receiving wild-type (WT) Sca-1^{+} BM cells and mice receiving caspase-1(Casp1)$^{-/-}$ Sca-1^{+} BM cells. The numbers shown indicate the numbers of mice in the group. E. Heart, Lung, Liver weight/body weight. The ratios of heart weight/body weight, lung weight/body weight and liver weight/body weight of mice receiving cell therapy and control mice.

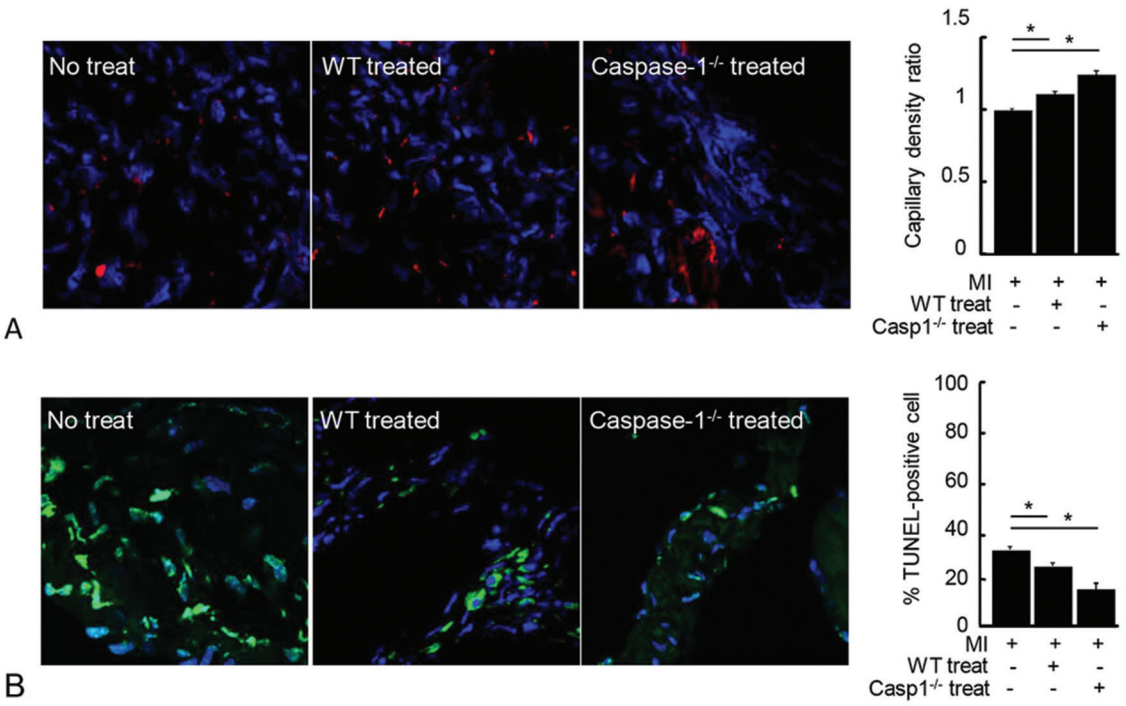

Figure 6. Caspase-1$^{-/-}$ Sca-1^{+} progenitor cell therapy increases IB4+ capillary density and decreases TUNEL+ cardiomyocytes. A. Capillary density detected with IB4 staining for endothelial cells in neovasculature. Histochemical analysis of heart cross sections showed that cell therapy with Sca-1^{+} BM cells from casp-1$^{-/-}$ mice increases IB4+ capillary density (endothelial cells) in comparison to the cell therapy with Sca-1^{+} BM cells from wild type (WT) mice. B. TUNEL Assay for detecting cell death in myocardial infarcted heart. Histochemical analysis of heart cross sections showed that the cell therapy with Sca-1^{+} BM cells from casp-1$^{-/-}$ mice decreases TUNEL+ cardiomyocytes in comparison to the cell therapy with Sca-1^{+} BM cells from WT mice.

5. DISCUSSION

Stem cell based therapies for the prevention and treatment of CVDs such as myocardial infarction have attracted considerable interest since it was reported in 2001 that BM-derived stem cells could repair myocardial infarcts in mice (27). Originally it was considered that stem cell therapies reverses myocardial remodeling by directly incorporate into the myocardium for de novo myocardiogenesis, it is believed today that the beneficial effects of stem cell therapy on ischemic myocardium are mainly due to neovascularization and paracrine effects (28). The results from clinical trials suggest that stem cell therapy for the prevention and treatment of cardiac dysfunction is safe and potentially efficacious, but the therapeutic efficacy of stem cell therapy is greatly hampered by poor survival, proliferation, engraftment, and differentiation of the grafted stem cells due to the hostile microenvironment of ischemic tissue such as hyperlipidemia, hypoxia, and inflammation (29,30). To overcome these limitations, a number of studies utilized genetic engineering and pharmacological approaches to empower stem cells for myocardial regeneration (31). However, three important questions remained poorly determined: *first*, whether progenitor cells have a functional caspase-1 pathway in sensing dyslipidemia/hyperlipidemia; *second*, whether caspase-1 induced cell death pathways including pyroptosis, apoptosis, and necrosis weaken angiogenesis and vascular repair function of progenitor cells after hyperlipidemia stimulation; and *third*, whether inhibition of caspase-1 in progenitor cells improves their angiogenesis capacity after MI. In this report, by using various techniques including immunological, biochemical, microarray analysis followed by bioinformatics analysis, gene deficient mice, cell therapy, experimental MI model, and mouse cardiac function assessment, we have made the following important findings: *1)* Dyslipidemia increases caspase-1 activity in Sca-1^{+} progenitor cells; *2)* Caspase-1 gene deficiency significantly reversed hyperlipidemia-induced gene changes in mouse aortas including progenitor cells, some of which are involved in vascular cell death; *3)* Caspase-1$^{-/-}$ Sca-1^{+} progenitor cell therapy significantly improves mouse cardiac functions after MI compared to the Sca-1^{+} progenitor cell treatment; and *4)* Caspase-1$^{-/-}$ Sca-1^{+} progenitor cell therapy improves capillary endothelial cell density and decrease cardiomyocyte cell death after MI. Taken together, our novel findings have provided the first insight on the role of dyslipidemia as DAMP in promoting caspase-1 dependent impairment of progenitor cell repairing capacity after MI.

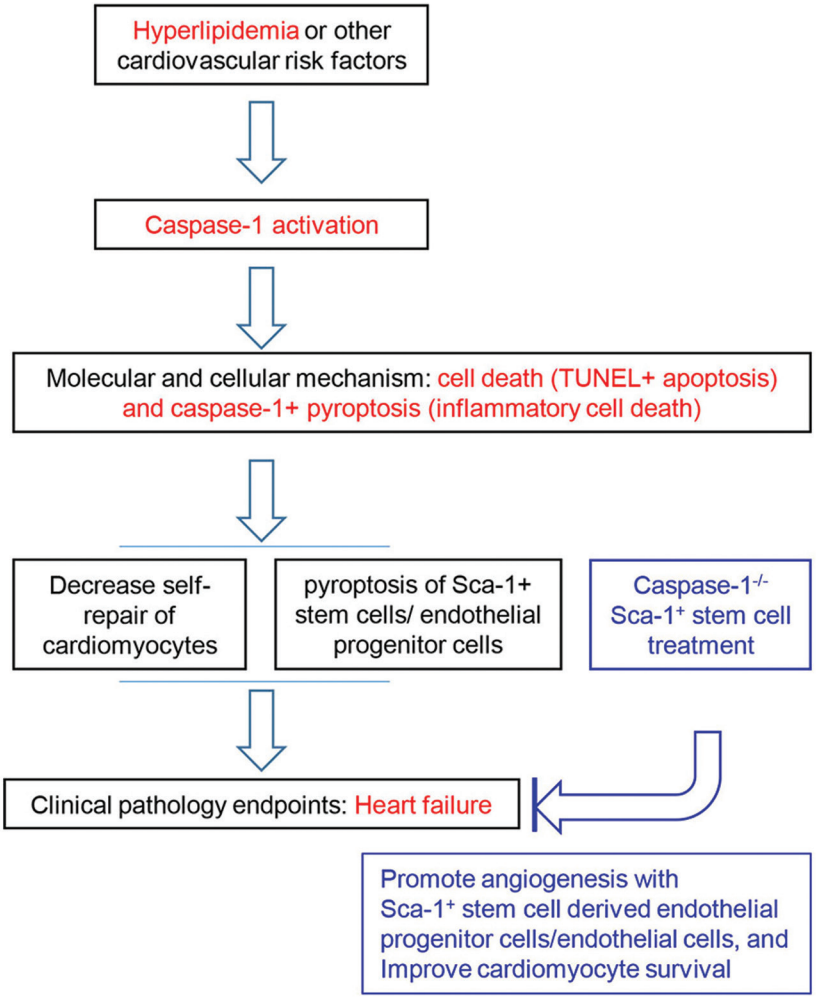

Figure 7. A new working model that caspase-1 inhibition improves Sca-1$^+$ stem cell therapy for myocardial infarction. Hyperlipidemia activates caspase-1 activation in Sca-1$^+$ stem cells and vascular cells in aorta. Activation of caspase-1 upregulates proinflammatory gene expression and promotes pyroptosis and apoptosis presumably in Sca-1$^+$ stem cells, endothelial cells and cardiomyocytes and causes cardiac dysfunction. Inhibition/depletion of caspase-1 improves survival of Sca-1$^+$ stem cells/progenitor cells, and cardiomyocytes, promotes angiogenesis, and improves cardiac function after myocardial infarction.

As we pointed out in our recent review, several types of inflammasomes involved in activating caspase-1 have been characterized including NLRP1, NLRP3, NLRC4 (IPAF), NFLRP6 and NLRP12 (12). Among these, the NLRP3 inflammasome is the only one found to activate caspase-1 in response to endogenous metabolic danger signals (DAMPs) including lipid metabolites. Nevertheless, future work is needed to verify the role of NLRP3 inflammasome in activating caspase-1 in Sca-1$^+$ progenitor cells. A previous report showed that inhibition of caspase-1 in BM-derived progenitor cells from patients and mice with systemic lupus erythematosus improves their differentiation ability (32). However, the questions related to caspase-1 activation in progenitor cells in response to dyslipidemia and its effects on angiogenesis and vascular repair after MI have not been examined until this study.

In addition to the phenotypic characterization of caspase-1$^{-/-}$ Sca-1$^+$ progenitor cell therapy for MI, we have also made the findings that after MI, caspase-1$^{-/-}$ Sca-1$^+$ progenitor cells improved capillary density and enhanced cardiomyocyte survival after MI, which are the mechanisms underlying the better efficiencies of caspase-1$^{-/-}$ Sca-1$^+$ progenitor cell therapy and better cardiac function in comparison to that of WT Sca-1$^+$ progenitor cells. Since that caspase-1 is the converting enzyme responsible for the maturation of pro-interleukin-1β (pro-IL-1β) and pro-IL-18 into IL-1β and IL-18, respectively (33); and that caspase-1 deficiency results in deficiency of functional IL-1β and IL-18 and decreased secretion of tumor necrosis factor-α (TNF-α)(12), there might be less proinflammatory cytokines IL-1β, IL-18 and TNF-α in the downstream of caspase-1 activation, resulting in improved vessel repair ability in the caspase-1$^{-/-}$ Sca-1$^+$

progenitor cells. Finally, we and others have reported previously that Sirtuin 1 (Sirt1), an inhibitory NAD+-dependent histone deacetylase, is cleaved by caspase-1 after hyperlipidemia stimulation (4,34). Disruption of Sirt1 gene results in defective blood vessel formation and inhibits ischemia-induced neovascularization (35). Thus, caspase-1$^{-/-}$ Sca-1^{+} progenitor cells might retain the Sirt1 function, which may also benefit ischemia-induced neovascularization during MI. Based on these analyses, we have proposed a new working model to integrate our findings (Figure 7). In summary, our results hold a promise for the future development of caspase-1 inhibitory progenitor cell therapy for inflammatory diseases, ischemic diseases, and cancers.

6. ACKNOWLEDGEMENTS

Ya-Feng Li, Xiao Huang, Xinyuan Li, contributed equally to the work. There is no conflict of interest by the authors. We are very grateful to Dr. Richard Flavell in the Department of Immunobiology at Yale University School of Medicine for generously providing us caspase-1 gene knock-out mice and Dr. Andrew Van Praagh at Carestream Molecular Imaging for the fluorescence-labeling of Sca-1^{+} BM cells. We would also like to thank Dr. Barrie Ashby in Temple University School of Medicine for critical reading. This work was partially supported by the National Institutes of Health Grants to HW and XFY.

7. REFERENCES

1. P. Libby, P. M. Ridker and G. K. Hansson: Progress and challenges in translating the biology of atherosclerosis. *Nature*, 473(7347), 317-25 (2011) DOI: 10.1038/nature10146
2. J. Mestas and K. Ley: Monocyte-endothelial cell interactions in the development of atherosclerosis. *Trends Cardiovasc Med*, 18(6), 228-32 (2008) DOI: 10.1016/j.tcm.2008.11.004
3. X. Jiang, F. Yang, H. Tan, D. Liao, R. M. Bryan, Jr., J. K. Randhawa, R. E. Rumbaut, W. Durante, A. I. Schafer, X. Yang and H. Wang: Hyperhomocystinemia impairs endothelial function and eNOS activity via PKC activation. *Arterioscler Thromb Vasc Biol*, 25(12), 2515-21 (2005) DOI: 10.1161/01.ATV.0000189559.87328.e4
4. Y. Yin, X. Li, X. Sha, H. Xi, Y. F. Li, Y. Shao, J. Mai, A. Virtue, J. Lopez-Pastrana, S. Meng, D. Tilley, M. A. Monroy, E. T. Choi, C. J. Thomas, X. Jiang, H. Wang and X. F. Yang: Early Hyperlipidemia Promotes Endothelial Activation via a Caspase-1-Sirtuin 1 Pathway. *Arterioscler Thromb Vasc Biol* (2015) DOI: 10.1161/ATVBAHA.115.305282
5. D. Zhang, X. Jiang, P. Fang, Y. Yan, J. Song, S. Gupta, A. I. Schafer, W. Durante, W. D. Kruger, X. Yang and H. Wang: Hyperhomocysteinemia promotes inflammatory monocyte generation and accelerates atherosclerosis in transgenic cystathionine beta-synthase-deficient mice. *Circulation*, 120(19), 1893-902 (2009) DOI:10.1161/CIRCULATIONAHA.109.866889
6. C. Combadiere, S. Potteaux, M. Rodero, T. Simon, A. Pezard, B. Esposito, R. Merval, A. Proudfoot, A. Tedgui and Z. Mallat: Combined inhibition of CCL2, CX3CR1, and CCR5 abrogates Ly6C(hi) and Ly6C(lo) monocytosis and almost abolishes atherosclerosis in hypercholesterolemic mice. *Circulation*, 117(13), 1649-57 (2008) DOI:10.1161/CIRCULATIONAHA.107.745091
7. D. Zhang, P. Fang, X. Jiang, J. Nelson, J. K. Moore, W. D. Kruger, R. M. Berretta, S. R. Houser, X. Yang and H. Wang: Severe hyperhomocysteinemia promotes bone marrow-derived and resident inflammatory monocyte differentiation and atherosclerosis in LDLr/CBS-deficient mice. *Circ Res*, 111(1), 37-49 (2012) DOI: 10.1161/CIRCRESAHA.112.269472
8. P. Fang, D. Zhang, Z. Cheng, C. Yan, X. Jiang, W. D. Kruger, S. Meng, E. Arning, T. Bottiglieri, E. T. Choi, Y. Han, X. F. Yang and H. Wang: Hyperhomocysteinemia potentiates hyperglycemia-induced inflammatory monocyte differentiation and atherosclerosis. *Diabetes*, 63(12), 4275-90 (2014) DOI: 10.2337/db14-0809
9. Z. Xiong, Y. Yan, J. Song, P. Fang, Y. Yin, Y. Yang, A. Cowan, H. Wang and X. F. Yang: Expression of TCTP antisense in CD25(high) regulatory T cells aggravates cuff-injured vascular inflammation. *Atherosclerosis*, 203(2), 401-8 (2009) DOI: 10.1016/j.atherosclerosis.2008.07.041
10. H. Ait-Oufella, B. L. Salomon, S. Potteaux, A. K. Robertson, P. Gourdy, J. Zoll, R. Merval, B. Esposito, J. L. Cohen, S. Fisson, R. A. Flavell, G. K. Hansson, D. Klatzmann, A. Tedgui and Z. Mallat: Natural regulatory T cells control the development of atherosclerosis in mice. *Nat*

Med, 12(2), 178-80 (2006)
DOI: 10.1038/nm1343

11. F. Du, J. Zhou, R. Gong, X. Huang, M. Pansuria, A. Virtue, X. Li, H. Wang and X. F. Yang: Endothelial progenitor cells in atherosclerosis. *Front Biosci*, 17, 2327-49 (2012)
DOI: 10.2741/4055

12. Y. Yin, J. L. Pastrana, X. Li, X. Huang, K. Mallilankaraman, E. T. Choi, M. Madesh, H. Wang and X. F. Yang: Inflammasomes: sensors of metabolic stresses for vascular inflammation. *Front Biosci (Landmark Ed)*, 18, 638-49 (2013)
DOI: 10.2741/4127

13. C. E. Ford, M. Faedo, R. Crouch, J. S. Lawson and W. D. Rawlinson: Progression from normal breast pathology to breast cancer is associated with increasing prevalence of mouse mammary tumor virus-like sequences in men and women. *Cancer Res*, 64(14), 4755-9 (2004)
DOI: 10.1158/0008-5472.CAN-03-3804

14. P. Duewell, H. Kono, K. J. Rayner, C. M. Sirois, G. Vladimer, F. G. Bauernfeind, G. S. Abela, L. Franchi, G. Nunez, M. Schnurr, T. Espevik, E. Lien, K. A. Fitzgerald, K. L. Rock, K. J. Moore, S. D. Wright, V. Hornung and E. Latz: NLRP3 inflammasomes are required for atherogenesis and activated by cholesterol crystals. *Nature*, 464(7293), 1357-61 (2010)
DOI: 10.1038/nature08938

15. K. Rajamaki, J. Lappalainen, K. Oorni, E. Valimaki, S. Matikainen, P. T. Kovanen and K. K. Eklund: Cholesterol crystals activate the NLRP3 inflammasome in human macrophages: a novel link between cholesterol metabolism and inflammation. *PLoS One*, 5(7), e11765 (2010)
DOI: 10.1371/journal.pone.0011765

16. Y. Yin, Y. Yan, X. Jiang, J. Mai, N. C. Chen, H. Wang and X. F. Yang: Inflammasomes are differentially expressed in cardiovascular and other tissues. *Int J Immunopathol Pharmacol*, 22(2), 311-22 (2009)
No DOI Found

17. K. Kuida, J. A. Lippke, G. Ku, M. W. Harding, D. J. Livingston, M. S. Su and R. A. Flavell: Altered cytokine export and apoptosis in mice deficient in interleukin-1 beta converting enzyme. *Science*, 267(5206), 2000-3 (1995)
DOI: 10.1126/science.7535475

18. E. Gao, Y. H. Lei, X. Shang, Z. M. Huang, L. Zuo, M. Boucher, Q. Fan, J. K. Chuprun, X. L. Ma and W. J. Koch: A novel and efficient model of coronary artery ligation and myocardial infarction in the mouse. *Circ Res*, 107(12), 1445-53 (2010)
DOI: 10.1161/CIRCRESAHA.110.223925

19. J. N. Rottman, G. Ni and M. Brown: Echocardiographic evaluation of ventricular function in mice. *Echocardiography*, 24(1), 83-9 (2007)
DOI: 10.1111/j.1540-8175.2006.00356.x

20. E. Chavakis, A. Aicher, C. Heeschen, K. Sasaki, R. Kaiser, N. El Makhfi, C. Urbich, T. Peters, K. Scharffetter-Kochanek, A. M. Zeiher, T. Chavakis and S. Dimmeler: Role of beta2-integrins for homing and neovascularization capacity of endothelial progenitor cells. *J Exp Med*, 201(1), 63-72 (2005)
DOI: 10.1084/jem.20041402

21. J. S. Russell and J. M. Brown: Circulating mouse Flk1+/c-Kit+/CD45- cells function as endothelial progenitors cells (EPCs) and stimulate the growth of human tumor xenografts. *Mol Cancer*, 13, 177 (2014)
DOI: 10.1186/1476-4598-13-177

22. A. S. Plump, J. D. Smith, T. Hayek, K. Aalto-Setala, A. Walsh, J. G. Verstuyft, E. M. Rubin and J. L. Breslow: Severe hypercholesterolemia and atherosclerosis in apolipoprotein E-deficient mice created by homologous recombination in ES cells. *Cell*, 71(2), 343-53 (1992)
DOI: 10.1016/0092-8674(92)90362-G

23. Y. Nakashima, A. S. Plump, E. W. Raines, J. L. Breslow and R. Ross: ApoE-deficient mice develop lesions of all phases of atherosclerosis throughout the arterial tree. *Arterioscler Thromb*, 14(1), 133-40 (1994)
DOI: 10.1161/01.ATV.14.1.133

24. H. Iwasaki, A. Kawamoto, M. Ishikawa, A. Oyamada, S. Nakamori, H. Nishimura, K. Sadamoto, M. Horii, T. Matsumoto, S. Murasawa, T. Shibata, S. Suehiro and T. Asahara: Dose-dependent contribution of CD34-positive cell transplantation to concurrent vasculogenesis and cardiomyogenesis for functional regenerative recovery after myocardial infarction. *Circulation*, 113(10), 1311-25 (2006)
DOI:10.1161/CIRCULATIONAHA.105.541268

25. J. Chen, H. Li, F. Addabbo, F. Zhang, E. Pelger, D. Patschan, H. C. Park, M. C. Kuo, J. Ni, G. Gobe, P. N. Chander, A. Nasjletti and M. S. Goligorsky: Adoptive transfer of syngeneic bone marrow-derived cells in mice with obesity-induced diabetes: selenoorganic antioxidant ebselen restores stem cell competence. *Am J Pathol*, 174(2), 701-11 (2009)
DOI: 10.2353/ajpath.2009.080606

26. M. Scherrer-Crosbie and H. B. Thibault: Echocardiography in translational research: of mice and men. *J Am Soc Echocardiogr*, 21(10), 1083-92 (2008)
DOI: 10.1016/j.echo.2008.07.001

27. D. Orlic, J. Kajstura, S. Chimenti, D. M. Bodine, A. Leri and P. Anversa: Transplanted adult bone marrow cells repair myocardial infarcts in mice. *Ann N Y Acad Sci*, 938, 221-9; discussion 229-30 (2001)
DOI: 10.1111/j.1749-6632.2001.tb03592.x

28. T. Kinnaird, E. Stabile, M. S. Burnett, M. Shou, C. W. Lee, S. Barr, S. Fuchs and S. E. Epstein: Local delivery of marrow-derived stromal cells augments collateral perfusion through paracrine mechanisms. *Circulation*, 109(12), 1543-9 (2004)
DOI: 10.1161/01.CIR.0000124062.31102.57

29. M. S. Penn and A. A. Mangi: Genetic enhancement of stem cell engraftment, survival, and efficacy. *Circ Res*, 102(12), 1471-82 (2008)
DOI: 10.1161/CIRCRESAHA.108.175174

30. X. F. Yang: Immunology of stem cells and cancer stem cells. *Cell Mol Immunol*, 4(3), 161-71 (2007)
No DOI Found

31. S. Mohsin, S. Siddiqi, B. Collins and M. A. Sussman: Empowering adult stem cells for myocardial regeneration. *Circ Res*, 109(12), 1415-28 (2011)
DOI: 10.1161/CIRCRESAHA.111.243071

32. J. M. Kahlenberg, S. G. Thacker, C. C. Berthier, C. D. Cohen, M. Kretzler and M. J. Kaplan: Inflammasome activation of IL-18 results in endothelial progenitor cell dysfunction in systemic lupus erythematosus. *J Immunol*, 187(11), 6143-56 (2011)
DOI: 10.4049/jimmunol.1101284

33. J. Shen, Y. Yin, J. Mai, X. Xiong, M. Pansuria, J. Liu, E. Maley, N. U. Saqib, H. Wang and X. F. Yang: Caspase-1 recognizes extended cleavage sites in its natural substrates. *Atherosclerosis*, 210(2), 422-9 (2010)
DOI: 10.1016/j.atherosclerosis.2009.12.017

34. A. Chalkiadaki and L. Guarente: High-fat diet triggers inflammation-induced cleavage of SIRT1 in adipose tissue to promote metabolic dysfunction. *Cell Metab*, 16(2), 180-8 (2012)
DOI: 10.1016/j.cmet.2012.07.003

35. M. Potente, L. Ghaeni, D. Baldessari, R. Mostoslavsky, L. Rossig, F. Dequiedt, J. Haendeler, M. Mione, E. Dejana, F. W. Alt, A. M. Zeiher and S. Dimmeler: SIRT1 controls endothelial angiogenic functions during vascular growth. *Genes Dev*, 21(20), 2644-58 (2007)
DOI: 10.1101/gad.435107

Key Words: Stem cell therapy, Myocardial infarction, Angiogenesis, Caspase-1 activation, Hyperlipidemia

Send correspondence to: Cong-xin Huang, No. 238, Jiefang Road, Wuchang District, Wuhan City, Hubei Province, PR China, Tel: 86-027-88041911, Fax: 86-027-88041911, E-mail: huangcongxin1951@163.com